ACS Photonics

Article

pubs.acs.org/journal/apchd5

Necklace State Hallmark in Disordered 2D Photonic Systems

Fabrizio Sgrignuoli,*[,†,‡] Giacomo Mazzamuto,[‡,§] Niccolò Caselli,[†,§] Francesca Intonti,[†,§] Francesco Saverio Cataliotti,[†,§,⊥] Massimo Gurioli,[†,§] and Costanza Toninelli[‡,§,⊥]

[†]Dipartimento di Fisica ed Astronomia, Università di Firenze, Via Sansone 1, I-50019 Sesto F.no, Firenze, Italy

[‡]CNR-INO, Istituto Nazionale di Ottica, Via Carrara 1, 50019 Sesto F.no, Firenze, Italy

[§]LENS and Università di Firenze, Via Carrara 1, 50019 Sesto F.no, Firenze, Italy

[⊥]QSTAR, Largo Fermi 2, I-50125 Firenze, Italy

Supporting Information

ABSTRACT: Necklace states arise from the coupling of otherwise confined modes in disordered photonic systems and open high transmission channels in strongly scattering media. Despite their potential relevance in the transport properties of photonic systems, necklace state statistical occurrence in dimensions higher than one is hard to measure, because of the lack of a decisive signature. In this work we provide an efficient method to tell apart in a single measurement a coupled mode from a single localized state in a complex scattering problem, exploiting the analogy with well-characterized coupled cavities in photonic crystals. The phase spatial distribution of the electromagnetic field has been numerically calculated and analyzed as a function of the coupling strength and of detuning between interacting modes respectively for coupled photonic crystal cavities and for partially disordered systems. Results consistently show that when localized modes spectrally and spatially overlap only over a small surface extent, synchronous oscillation does not build up and the phase spatial distribution splits into two distinct peaks. Having established such bimodal distribution as a necklace hallmark, this paper opens the possibility to assess and eventually tailor the role of necklace states in random systems, e.g., by varying correlations.

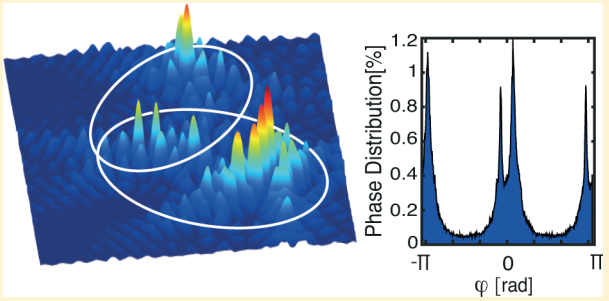

KEYWORDS: *necklace states, partially disordered 2D systems, photonic nanocavities*

Transport properties in complex systems depend critically on the interplay between disorder, correlations, and interaction. Communication, i.e., transport of information through physical carriers, is described in the same parameter space. Photons are ideal candidates for this purpose, for both fundamental and practical reasons. Indeed, they are inherently characterized by a negligible interaction cross section, and well-established technologies, from self-assembly to the most complex lithographic processes, enable efficient manipulation of the light flow in artificial photonic structures.[1]

Photonic crystal fibers are perhaps the first example of a commercial product along this line. Fabrication imperfections however induce unwanted scattering and hinder performances, typically determining an upper bound to the propagation length in one-dimensional photonic waveguides.[2,3] However, scattering of light should not be regarded as a simple linear loss channel. As thoroughly discussed in ref 4, propagation is inhibited as the sample length exceeds a critical length scale, dubbed localization length, because of the forming of trap states through interference. This phenomenology is related to the halt of diffusion determined by the localization of the electronic wave function in certain semiconductors.[5] Such an apparently detrimental factor has been exploited, e.g., by Sapienza and co-workers, to modify the optical properties of solid-state quantum emitters coupled to confined optical modes in 1D disordered systems,[6] suggesting that Anderson localized modes might offer an unconventional platform for cavity quantum electrodynamics applications. As a matter of fact, the progress in optical communications relies on the understanding of transport mechanisms in the presence of disorder.

Consider, as an example, the case of light control on a chip, in two-dimensional photonic crystal structures, affected by random imperfections. Due to the strong dispersion in the density of states, disorder induces the formation of localized modes preferentially at the band edge.[7] The transport properties are strongly related to the nature of such states. Indeed, in the language of eigenchannel statistics, localization corresponds to the single-channel regime,[8] where every transmission channel is univocally related to the formation of a quasi-mode in the structure.[9] Interestingly, these states can be either single localized ones, featuring exponentially decaying tails, or multipeaked states, formed by the hybridization of two or more separate modes. Besides robust confinement, the complexity of light transport allowing for high transmission

Received: July 29, 2015
Published: October 19, 2015

DOI: 10.1021/acsphotonics.5b00422
ACS Photonics 2015, 2, 1636−1643

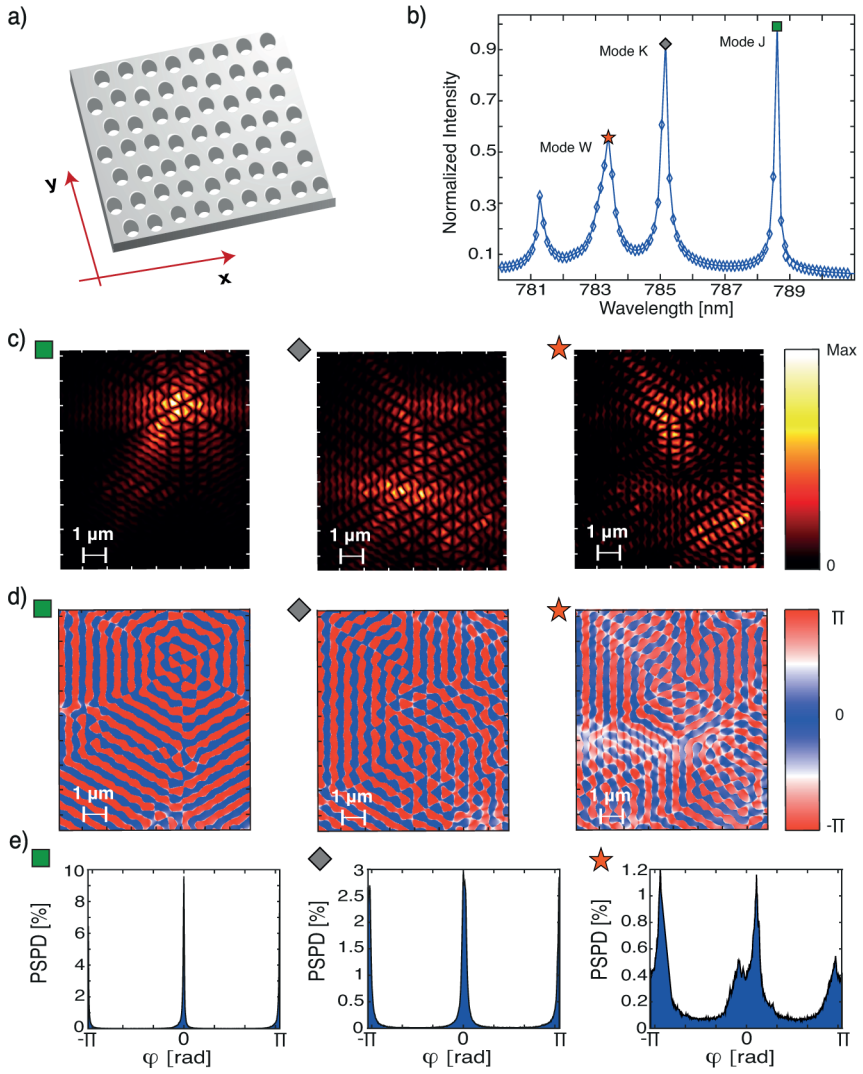

Figure 1. (a) Schematic view of the nanostructured film with Gaussian disorder in the hole positions. (b) FDTD intensity spectrum for the H_z field component of a typical 2D disordered configuration. (c) Spatial distribution of the amplitude for the H_z field component of three modes, labeled J (λ_J = 788.6 nm), K (λ_K = 785.1 nm), and W (λ_W = 783.4 nm), identified by a green square, a gray diamond, and a red star in spectrum b, respectively. (d and e) Phase map and spatial probability distribution of the phase for modes J, K, and W, respectively.

channels generally impacts the connectivity between distant points, defined as the number of eigenchannels connecting them.[10]

The occurrence of so-called necklace states was originally predicted by Pendry,[11] then observed in time-resolved experiments[12] and by measuring cumulative phase lag of the transmitted light field[13] in one-dimensional systems. In 2D however, where the output in transmission is a complex speckle pattern, phase lag is not easily defined and a different approach is required to single out coupled modes. Such states in 2D disordered structures have been experimentally induced and monitored by means of a local control of the refractive index, which gradually varied the coupling strength.[14] However, the probability of their natural occurrence is not yet known, especially because of the lack of a decisive signature, enabling a statistical study over ensembles of configurations. Information about spectra, even if spatially resolved, is indeed not sufficient for this purpose, since two modes that are accidentally resonant cannot be discriminated from a single more extended mode. In ref 15 the phase spatial probability distribution has been suggested as a key to the problem, although remaining a single case study.

Here we present an extensive numerical analysis and data interpretation for the connectivity of an integrated optical system, where scattering occurs in 2D photonic crystals with a small amount of disorder. In particular, we define and test an indicator that combines the near-field spectral information with the phase spatial probability distribution, allowing the assessment of necklace states on a very general basis. It will hence enable extracting the internal coupling/transport mechanism of complex modes in the localized regime from a single static measurement of the field distribution. Our work provides a general result, which is not restricted to a small sample size and does not depend on the specific type of disorder or degree of correlations.

TRANSPORT THROUGH HYBRID MODES IN 2D DISORDERED PHOTONIC CRYSTALS

Let us consider a 230 nm thick photonic crystal (PhC) membrane of air holes arranged in a triangular lattice with lattice constant 325.5 nm and lateral dimension 12.1 × 13.7

DOI: 10.1021/acsphotonics.5b00422
ACS Photonics 2015, 2, 1636−1643

μm^2, made of Si_3N_4, hence characterized by a refractive index of 2.1 and vanishing absorption in the near infrared around 800 nm. Disorder is introduced in a controlled manner by shifting the holes' position by a small, normally distributed, displacement with respect to the position of the perfect periodic lattice, with a given σ, measured in units of the lattice constant. Enhanced multiple scattering with respect to an equivalent system without the underlying periodic backbone[16] induces the formation of localized modes at random positions in space but in a restricted frequency range, i.e., near the photonic band edges, where the density of states is higher.[4,7,17] We have considered disordered platforms with σ = 5%. This value guarantees an optimal interplay between order and disorder. Simulations were performed studying the dependence of the cavity-like quality factor Q on the amount of disorder: modes appear near the photonic band edge in a controllable fashion, with the highest Q values appearing closer to the photonic gap. Furthermore, Q values decrease, increasing the disorder σ from 1% to 5%, pulling the modes inside the band gap. On the other hand, σ values lower than 5% generate modes very similar to the Bloch ones, not enabling the typical mode description for random systems. In the chosen configuration, modes result from multiple scattering and hence occur at unpredictable positions, making the structure behave as a disordered one for our purposes.

A schematic of the disordered nanostructured film with a pore diameter size of 102 nm is reported in Figure 1a. The electromagnetic field is confined in the orthogonal direction due to the discontinuity in the dielectric function, whereas the average periodic arrangement of holes in a triangular lattice defines the photonic band gap in the xy-plane.

Mimicking a relevant experimental configuration, we probe the quasi-modes of this structure by continuous excitation of dipolar sources, parallel oriented and randomly located in the azimuthal plane. From the time-dependent response of the electromagnetic field after the dipoles have been switched off, we extract the spectral response of the system in any point of the structure by a Fourier transform analysis, yielding an amplitude $(A(x, y, \lambda)_z)$ and a phase $(\Phi(x, y, \lambda)_z)$ map for each wavelength (λ). The subscript z refers to the H_z polarization of the electromagnetic field. The normalized spectral response $(I_N(\lambda))$ of a 2D photonic structure, shown in Figure 1b, is defined as the integral

$$I(\lambda) = \iint A(x, y, \lambda)\, dx\, dy \tag{1}$$

where the normalization is performed with respect to the maximum value of $I(\lambda)$, i.e., $I_N(\lambda) = I(\lambda)/\max(I(\lambda))$. More details about the simulation methods are given in the Supporting Information.

Several modes, with a high degree of spatial localization, are identified by the peaks in Figure 1b. In Figure 1c we report the spatial distribution of the amplitude for the H_z field component of three different modes, labeled J, K, and W, corresponding to the green square (λ_J = 788.6 nm), gray diamond (λ_K = 785.1 nm), and red star marker (λ_W = 783.4 nm) in the calculated intensity spectrum (Figure 1b). It is worth noting that, although these simulations require the combination of high spatial and spectral resolution, the extracted information would not be sufficient to tell the dynamics of transport for different calculated photonic modes. Indeed, the mode J has a quality factor of ~5700, defined as $Q = \lambda_{peak}/\Delta\lambda$ (λ_{peak} and $\Delta\lambda$ identify the peak spectral position and the full width at half-maximum, respectively), while the mode K and the mode W have similar Q values (~2800 and ~2400, respectively). In order to estimate the spatial extent of the photonic mode, we use the inverse participation ratio as defined in ref 18:

$$R_{IP} = \frac{\int |\mathbf{H}(\mathbf{r})|^4 d^2r}{(\int |\mathbf{H}(\mathbf{r})|^2 d^2r)^2} \tag{2}$$

where the integral is performed over the detector plane, while $\mathbf{H}$ expresses the magnetic field. In particular, mode J is very localized, i.e., $1/R_{IP} \approx 1.5\ \mu m^2$. On the other hand, concerning modes K and W, we find similar spatial extents of $1/R_{IP} \approx 5.3\ \mu m^2$ and $1/R_{IP} \approx 6.7\ \mu m^2$ for the λ_K = 785.1 nm and λ_W = 783.4 nm resonance, respectively. However, as we will demonstrate below, light at 785.1 nm tunnels through a single mode, whereas transport at 783.4 nm relies on a two-step process, more similar to what would happen in a network of connected nodes. When the state results from the hybridization of two originally isolated modes, another time scale adds to the resonance lifetime $\tau = 1/\Gamma$ and that is the inverse of the coupling constant g. Note that, in the limiting case of $g \gg \Gamma$, strong coupling occurs and the state recovers a single-mode character, although spatially extended over a superposition of the uncoupled field profiles. The difference in quality factors and spatial extents associated with these three states is not surprising and reflects the statistical character of the multiple scattering underlying phenomenon.

In order to spot the different behaviors, we analyze not only the amplitude but also the spatial phase map and extract its spatial probability distribution, as shown in Figure 1d and e. As pointed out in ref 15, the probability distribution of detecting a certain phase is a complexity index, which turns out to be single-peaked for standing waves and broad for traveling waves. On the other hand, two weakly coupled modes ($g \lesssim \Gamma$), although oscillating at the same frequency (within the resonance spectral width), might be not synchronized, thus exhibiting a double peak in the phase distribution. Such distinct features are clearly visible in Figure 1e. In fact, the phase spatial probability distribution (PSPD) shows a single-peaked profile for the eigenmodes J and K (green square and gray diamond marker) or a double-peaked profile for the W resonance at 783.4 nm (red star marker).

Therefore, we raise the question: can the double-peaked phase profile be considered as a unique indicator of a transport mechanism based on a two-step process characterized by weakly coupled eigenmodes ? In this article, such a hypothesis is tested on a well-known system of coupled PhC-based nanocavities in which the coupling between resonant modes can be controlled. We then extend the concept to disordered structures, where we varied the spectral overlap between modes. Coherent results confirm the hypothesis here presented.

COUPLED PHOTONIC CRYSTALS CAVITIES: A TEST BED CONFIGURATION

Photonic crystal cavities (PCCs) are dielectric point defects in the photonic crystals' periodic lattice that generate electromagnetic localized states in the photonic band gaps.[1] Coupled PCCs are also denominated photonic crystal molecules (PCMs) due to the analogy with atomic states. The molecular-like interaction, characterized by an energy splitting of the normal modes,[19] is achieved by an evanescent tunneling between each single PCC resonant mode whenever the

DOI: 10.1021/acsphotonics.5b00422
ACS Photonics 2015, 2, 1636−1643

frequency matching and spatial overlap between them are fulfilled.[20−22]

Recently, a way to engineer the design of PCMs has been proposed allowing an accurate control of the ground-state parity.[23,24] The coupling constant g between the atomic modes can be tuned and even changed in sign by adjusting the hole diameter of the five central pores between two cavities, highlighted in green in Figure 2a. In more detail, this diameter

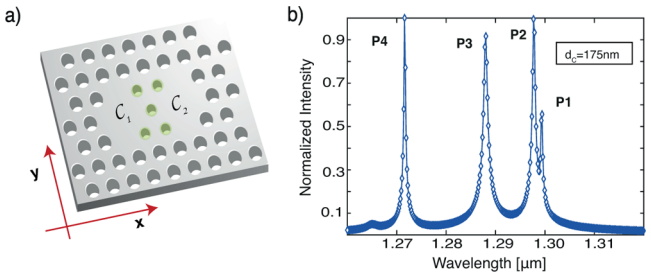

Figure 2. (a) Scheme of the modified PCM (in green, five central pores with reduced diameter 175 nm) used to tune the coupling strength between the two PCCs labeled C_1 and C_2. The K-axis is identified by the x-coordinate. (b) FDTD spectrum for the H_z field component of the system in panel a. It shows four fundamental modes. The label Pj was used to enumerate the four different eigenmodes with increasing index for decreasing wavelength.

reduction produces a continuous decrease of g, given by the overlap integral between the two atomic modes weighted over the dielectric function of the photonic system,[25] reaching the weakly coupling regime ($g \lesssim \Gamma$) and also a degenerate condition ($g \approx 0$).

Photonic Crystal Molecule Characterization. In order to test our conjecture about the phase behavior in the weak coupling regime, we have considered the same structure analyzed in ref 24: a 320 nm thick GaAs (n = 3.484) membrane with lateral dimensions of 7.2 × 7.3 μm^2. The photonic structure is composed by a two-dimensional triangular lattice of air holes with a lattice constant of 308 nm. The pores have a diameter of 193.2 nm, leading to a 35% filling fraction. The single cavity is formed by four missing holes, and it was largely characterized in ref 26. We have considered photonic molecules resulting from the coupling of two cavities (labeled C_1 and C_2) aligned along the principal K-axis of the photonic crystal, as shown in Figure 2a. We will use the labels M1 and M2 to indicate the two main modes of the single cavity.

Figure 2b reports the spectrum of the photonic structure depicted in panel a in which the five central holes' size was set equal to 175 nm. The label Pj was used to enumerate the four different eigenmodes with increasing index for decreasing wavelength. The pairs P1, P2 and P3, P4 can be modeled in term of two coupled oscillators with almost the same free frequency, whose interaction is mediated by the coupling strength g.[19,21] The molecular mode splitting between the lower and the excited state is given by $\sqrt{\Delta^2 + 4g^2}$, where Δ expresses the detuning.[19] Hence, assuming a vanishing detuning (nominally identical cavities), the wavelength splitting between the peaks P1, P2 and P3, P4 gives a direct estimation of the coupling strength absolute value. Each peak is a hybrid mode, whose spatial distribution is delocalized over the molecule[23] (for more details see also Figure 3). In particular, P1 and P2 modes result from a small but sizable coupling between the two M1 modes of C_1 and C_2. Whereas P3 and P4 are generated by the large coupling between the two M2 modes of the single

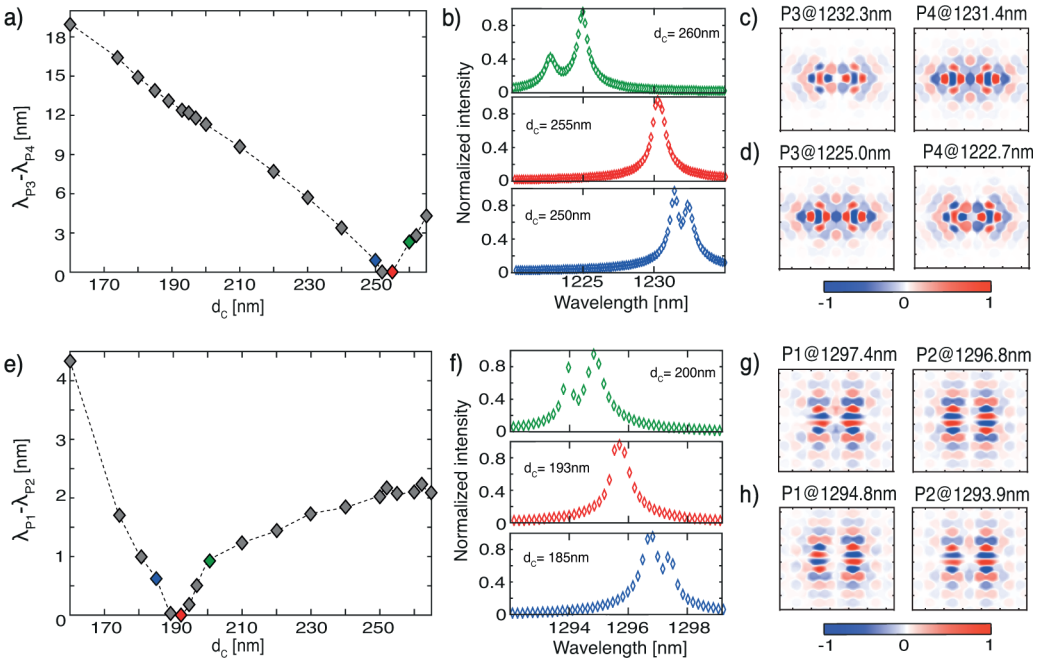

Figure 3. (a) Spectral shift of the peaks P3 and P4 as a function of the hole diameter of the five central pores (d_c). (b) Evolution of the resonant modes P3 and P4 near the degenerate point d_c = 255 nm (red curve) as a function of the wavelength (H_z field component shown). (c and d) Spatial distributions of the real part of the H_z component of P3 and P4 when d_c = 250 nm (blue curve in panel b) and d_c = 260 nm (green curve in panel b). (e and f) Spectral shift and the evolution for the H_z field component of the normalized intensity spectra near the degenerate point (d_c = 193 nm) of peaks P1 and P2. (g and h) Spatial distributions of the real part of the H_z component of the modes P1 and P2 before (d_c = 185 nm, blue curve in panel f) and after (d_c = 200 nm, green curve in panel f) the degenerate point.

DOI: 10.1021/acsphotonics.5b00422
ACS Photonics 2015, 2, 1636−1643

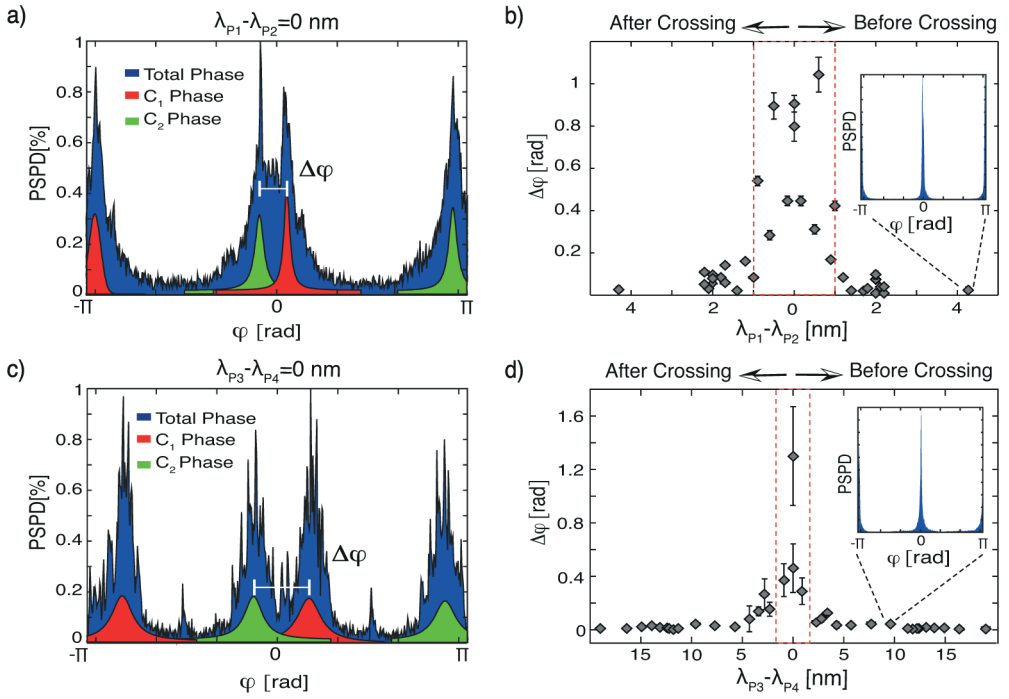

Figure 4. (a) Spatial probability distribution of the phase (PSPD) for the H_z field component of the modes P1 and P2 when d_c = 193 nm (degenerate condition) exhibiting a double-peaked profile. (b) Phase difference as a function of the wavelength splitting between the molecular modes P1 and P2 before and after the crossing point ($\lambda_{P1} - \lambda_{P2} = 0$). The inset shows the single-peaked PSPD corresponding to the strong coupling between the M1 modes of the two PCCs. (c) PSPD for the H_z field component of the peaks P3 and P4 corresponding to the weak coupling between the two M2 modes of C_1 and C_2, once more characterized by a double-peaked profile. (d) Phase difference relative to the molecular modes P3 and P4 before and after the crossing point ($\lambda_{P3} - \lambda_{P4} = 0$). The inset shows the single-peaked PSPD when the strong coupling regime is reached. The error bars are evaluated as the standard deviation between different fitting procedures. The red-dashed rectangles identify the space parameter in which $g \leq \Gamma$, i.e., the weak coupling zone. Note that the reported probability distributions have π-periodicity.

cavity. Indeed, due to the spatial properties of the modes M1 and M2,[26,27] the coupling between M1 modes is smaller with respect to the interaction between the field in M2, i.e., $\lambda_{P1} - \lambda_{P2}$ = 1.7 nm $\gtrsim \Delta\lambda$, while $\lambda_{P3} - \lambda_{P4}$ = 16.4 nm $\gg \Delta\lambda$, where $\Delta\lambda$ is the resonance line width, estimated to be on the order of 1 nm.

From Strong to Weak Coupling. Following the seminal work of ref 24 the dynamics of the four molecular-like modes is summarized in Figure 3. Let us now focus only on the dynamics of the resonant states P3 and P4. Starting from a modified pore diameter size (d_c) of 160 nm, corresponding to 19 nm of wavelength splitting, we observe that an increase of the central hole's diameter size produces a continuous decrease of the photonic coupling up to zero splitting (red diamond in Figure 3a). Indeed, the spectrum shows a single resonant mode for d_c = 255 nm, as evident from the red curve in Figure 3b, meaning that the photonic coupling is decreased down to a value below the mode broadening. This leads to a degeneracy of the P3 and P4 modes. With a further increase, a clear crossing is observed: the lower energy state P3 changes as a function of d_c. In more detail, Figure 3 panels c and d report the spatial distribution of the real part of the H_z component before (blue diamond marker in panel a) and after (green diamond marker in panel a) the degenerate point (red diamond marker in panel a): the field distribution of P3 and P4 interchanges passing through the degenerate condition. This is due to a dielectric-induced tuning. Moreover, increasing the holes' diameter size means subtracting dielectric material, accordingly with the observed blue shift of both modes. A local change of the dielectric environment in the central region between C_1 and C_2 produces a modification of the lower energy state. The evolution of the resonant modes P1 and P2 shows similar behavior (see Figure 3 bottom panels).[24]

Spatial Probability Distribution of the Phase as Indicator for the Different Coupling Regimes. We are now in the position to explore the PSPD both in the strong and in the weak coupling regime between nominally identical cavities. The phase distribution, calculated as described in the previous sections, shows a double-peaked profile when two PCC modes are weakly coupled (Figure 4a and c). On the other hand, it displays a single-peaked profile when the two PCC modes are strongly coupled, as shown in the insets of Figure 4panels b and d. Moreover, to identify each of the two components of the double-peaked profile, we have isolated the contribution of the two PCCs, evaluating the PSPD only on a rectangular detector centered on C_1 (red-shaded areas) and C_2 (green-shaded areas), respectively. A finite phase shift $\Delta\varphi$, equal to the distance between the two peaks forming the double-peaked profile (blue-shaded area), arises as the cavity modes are weakly coupled, i.e., in the range $g \leq \Gamma$. This leads to a double peak in the PSPD produced by the weak coupling of the two M1 modes (Figure 4a) and of the two M2 modes (Figure 4c) when the modified hole diameters are equal to 193 and 255 nm, respectively. On the contrary, the field oscillates in phase when the cavity modes are strongly coupled ($g \gg \Gamma$); hence a single peak appears in the PSPD for the P1 and P2 resonances (P3 and P4 peaks), as shown in the inset of Figure 4b (Figure 4d).

$\Delta\varphi$ as a function of the wavelength splitting between the molecular modes P1 and P2 (P3 and P4) is reported in Figure 4b (Figure 4d). The phase difference between the two single

DOI: 10.1021/acsphotonics.5b00422
ACS Photonics 2015, 2, 1636−1643

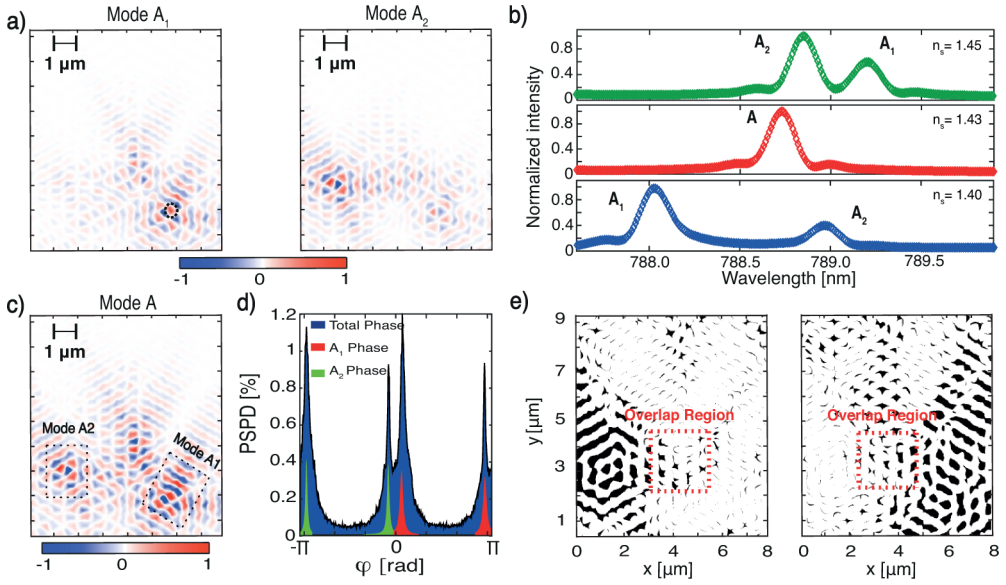

Figure 5. (a) Spatial distribution of the real part of the H_z field component for the two resonances, labeled A_1 and A_2 in the wavelength spectrum, reported in panel b, and corresponding to a local refractive index (n_s) of 1.4. The position of this scatterer, related to the maximum value of mode A_2, is marked by the black dashed circle. (b) Evolution of the H_z-normalized intensity spectra as a function of wavelength for n_s equal to 1.40 (blue curve), 1.43 (red curve), and 1.45 (green curve). (c, d, and e) Spatial distribution of the real part of the H_z field component, related to the phase probability distribution, and binary phase maps, when the crossing condition (n_s = 1.43) is met.

cavities becomes relevant only in a range in which the coupling constant is equal or lower with respect to the radiative losses (red dashed rectangle zone in the figures). In our case, $\Delta\varphi$ vanishes when the coupling constant exceeds Γ. Interestingly, in the weak coupling regime the phase lag $\Delta\varphi$ is finite but is not well-defined, as it strongly depends on the excitation or initial conditions. On the other hand, $\Delta\varphi$ is completely insensitive to initial conditions when the coupling constant increases.

In summary, two weakly coupled modes, although oscillating at the same frequency with some nonzero spatial overlap, are not synchronized; hence they exhibit a double-peaked profile in the spatial probability distribution of the phase.

SIGNATURES FOR HYBRID MODE FORMATION IN DISORDERED PHOTONIC CRYSTAL STRUCTURES

Let us now apply such numerical analysis to a disordered configuration that is different with respect to the one discussed in the second section. The difference is only in the arrangement of the air holes inside the membrane. Following the discussion of the previous sections, we make the hypothesis that a hybrid state results from the coupling of distinct localized ones and that this results in a double peak for the PSPD parameter. We further confirm this assumption by combining this information with the mode profile as a function of a controlled detuning of one of the modes with respect to the other. In particular, we locally change the refractive index of a single scatterer (n_s) around the maximum value of the field distribution (black dashed circle in Figure 5a). This single scatterer was varied from n_s = 1 to n_s = 2 with a step of 0.05. For each value of n_s, the procedure presented in the second section was applied. As most of the modes are localized away from the scatterer, they are insensitive to this local perturbation.

Nevertheless, Figure 5b shows the evolution for the H_z field component of the normalized intensity as a function of wavelength for two modes (A_1 and A_2) as a function of n_s. These two modes are spatially close and detuned in frequency (Figure 5a and blue curve in Figure 5b). A degenerate condition or a spectral overlap is observed for n_s = 1.43, corresponding to the red curve in Figure 5b. Increasing the dielectric perturbation (n_s = 1.45), the peak positions of modes A_1 and A_2 are inverted with respect to the situation depicted in Figure 5a: a crossing feature is observed between these two resonances.

This is demonstrated in the bottom panels of Figure 5. At the crossing condition, when n_s = 1.43, the spatial field distribution has a bilobated profile, clearly formed by the combination of mode A_1 and mode A_2 (Figure 5c). Moreover, the spatial probability distribution of the phase shows a double-peaked profile with a splitting of $\delta\phi = 0.4\pi$ (Figure 5d). In order to identify the underlying localized modes, we have calculated the phase contribution from two spatially isolated areas, identified with dashed rectangles in Figure 5c and reported as red- and green-shaded curves in panel d. The area of interest in modes A_1 and A_2 is clearly evident when we calculate the two binary phase maps reported in Figure 5e: black color denotes points with a phase between 0.44π and 0.57π and in the range $0.59-0.72\pi$ for modes A_1 and A_2, respectively. These two spatial distributions identify two distinct spatial regions associated with the standing components of the two modes, which oscillate at the same frequency but with a nonzero phase lag. Moreover, a small spatial overlap zone, compatible with the weak coupling condition, can be recognized in the red-highlighted area. This supports the picture of two weakly coupled eigenmodes, overlapping both spectrally and spatially, to form a hybrid state in which light transport relies on a two-step process. In analogy to the one-dimensional case, we dub these modes necklace states.

A similar analysis performed on mode K of the disordered configuration depicted in Figure 1 and reported in the Supporting Information confirms instead that a single peak in the spatial probability distribution corresponds to a shift without splitting of the spectrum upon perturbation.

DOI: 10.1021/acsphotonics.5b00422
ACS Photonics 2015, 2, 1636−1643

SUMMARY

In summary, this work numerically investigates the formation of localized and hybrid modes, due to symmetry breaking in partially disordered photonic crystals. In order to establish the role of so-called necklace states in the transport properties, we define a unique signature for weakly coupled modes, based on the near-field spatial distribution of the phase. This establishes a benchmark in the study of 2D disordered systems. The phase spatial probability distribution has been analyzed on a test bed architecture of coupled photonic nanocavities, as a function of their coupling strength. Similar results showing a double-peaked profile have been produced in a simulated experiment, where the relative detuning between isolated localized modes was brought to zero.

The method here discussed in order to assign a necklace state character from the phase spatial modulation of a given mode could be meaningfully extended to experimental cases. In fact, many near-field methods have shown high-resolution phase imaging in different nanoresonators, such as plasmonic nanorods and photonic crystal cavities.[28−30] These experimental methods exploit scattering scanning near-field optical microscopy in combination with pseudoheterodyne detection or with the analysis of the spatial modulation of Fano line shapes to retrieve the phase information along the sample surface. Therefore, they could be easily extended also to photonic modes localized in disordered systems, like the ones presented theoretically in our paper.

Our conclusions provide a tool to tell apart necklace states from single isolated modes and will be relevant to assess their role in the transition between diffusion and Anderson localization in random systems. Given the simplicity of the proposed analysis, a systematic study of necklace state occurrence as a function of correlations in random media can be envisaged.

ASSOCIATED CONTENT

Supporting Information

The Supporting Information is available free of charge on the ACS Publications website at DOI: 10.1021/acsphotonics.5b00422.

Details of the implemented simulation tool. Detuning analysis of the mode K introduced in the section Transport through Hybrid Modes in 2D Disordered Photonic Crystals (PDF)

AUTHOR INFORMATION

Corresponding Author

*Phone: +39 055-4572025. E-mail: sgrignuoli@lens.unifi.it.

Notes

The authors declare no competing financial interest.

ACKNOWLEDGMENTS

F.S. and F.S.C. acknowledge support from the Italian Ministry of University and Research through the "Futuro in Ricerca" project RBFR085XVZ-HYTEQ. C.T. and G.M. acknowledge support from the MIUR program Atom-Based Nanotechnology and from the Ente Cassa di Risparmio di Firenze with the project GRANCASSA. The authors also acknowledge Dr. F. Riboli, Dr. A. Trombettoni, Dr. G. Gori, and Prof. D. S. Wiersma for fruitful discussions.

REFERENCES

(1) Joannopoulos, J. D.; Johnson, S. G.; Winn, J. N.; Meade, R. D. *Photonic Crystals: Molding the Flow of Light*; Princeton University Press, 2011.

(2) Koenderink, A. F.; Lagendijk, A.; Vos, W. L. Optical extinction due to intrinsic structural variations of photonic crystals. *Phys. Rev. B: Condens. Matter Mater. Phys.* **2005**, *72*, 153102.

(3) Hughes, S.; Ramunno, L.; Young, J. F.; Sipe, J. Extrinsic optical scattering loss in photonic crystal waveguides: role of fabrication disorder and photon group velocity. *Phys. Rev. Lett.* **2005**, *94*, 033903.

(4) García, P.; Smolka, S.; Stobbe, S.; Lodahl, P. Density of states controls Anderson localization in disordered photonic crystal waveguides. *Phys. Rev. B: Condens. Matter Mater. Phys.* **2010**, *82*, 165103.

(5) Anderson, P. W. Absence of diffusion in certain random lattices. *Phys. Rev.* **1958**, *109*, 1492.

(6) Sapienza, L.; Thyrrestrup, H.; Stobbe, S.; Garcia, P. D.; Smolka, S.; Lodahl, P. Cavity quantum electrodynamics with Anderson-localized modes. *Science* **2010**, *327*, 1352−1355.

(7) John, S. Strong localization of photons in certain disordered dielectric superlattices. *Phys. Rev. Lett.* **1987**, *58*, 2486.

(8) Chabanov, A.; Stoytchev, M.; Genack, A. Statistical signatures of photon localization. *Nature* **2000**, *404*, 850−853.

(9) Peña, A.; Girschik, A.; Libisch, F.; Rotter, S.; Chabanov, A. The single-channel regime of transport through random media. *Nat. Commun.* **2014**, 510.1038/ncomms4488.

(10) Cazé, A.; Pierrat, R.; Carminati, R. Strong coupling to two-dimensional Anderson localized modes. *Phys. Rev. Lett.* **2013**, *111*, 053901.

(11) Pendry, J. Quasi-extended electron states in strongly disordered systems. *J. Phys. C: Solid State Phys.* **1987**, *20*, 733.

(12) Bertolotti, J.; Gottardo, S.; Wiersma, D. S.; Ghulinyan, M.; Pavesi, L. Optical necklace states in Anderson localized 1D systems. *Phys. Rev. Lett.* **2005**, *94*, 113903.

(13) Bertolotti, J.; Galli, M.; Sapienza, R.; Ghulinyan, M.; Gottardo, S.; Andreani, L.; Pavesi, L.; Wiersma, D. Wave transport in random systems: Multiple resonance character of necklace modes and their statistical behavior. *Phys. Rev. E* **2006**, *74*, 035602.

(14) Riboli, F.; Caselli, N.; Vignolini, S.; Intonti, F.; Vynck, K.; Barthelemy, P.; Gerardino, A.; Balet, L.; Li, L. H.; Fiore, A.; Gurioli, M.; Wiersma, D. Engineering of light confinement in strongly scattering disordered media. *Nat. Mater.* **2014**, *13*, 720−725.

(15) Vanneste, C.; Sebbah, P. Complexity of two-dimensional quasimodes at the transition from weak scattering to Anderson localization. *Phys. Rev. A: At., Mol., Opt. Phys.* **2009**, *79*, 041802.

(16) Toninelli, C.; Vekris, E.; Ozin, G. A.; John, S.; Wiersma, D. S. Exceptional reduction of the diffusion constant in partially disordered photonic crystals. *Phys. Rev. Lett.* **2008**, *101*, 123901.

(17) García, P. D.; Sapienza, R.; Toninelli, C.; López, C.; Wiersma, D. S. Photonic crystals with controlled disorder. *Phys. Rev. A: At., Mol., Opt. Phys.* **2011**, *84*, 023813.

(18) Mirlin, A. D. Statistics of energy levels and eigenfunctions in disordered systems. *Phys. Rep.* **2000**, *326*, 259−382.

(19) Cohen-Tannoudji, C.; Diu, B.; Laloë, F. *Quantum Mechanics*; Wiley, 1977.

(20) Bayer, M.; Gutbrod, T.; Reithmaier, J.; Forchel, A.; Reinecke, T.; Knipp, P.; Dremin, A.; Kulakovskii, V. Optical modes in photonic molecules. *Phys. Rev. Lett.* **1998**, *81*, 2582.

(21) Atlasov, K. A.; Karlsson, K. F.; Rudra, A.; Dwir, B.; Kapon, E. Wavelength and loss splitting in directly coupled photonic-crystal defect microcavities. *Opt. Express* **2008**, *16*, 16255−16264.

(22) Vignolini, S.; Intonti, F.; Zani, M.; Riboli, F.; Wiersma, D. S.; Li, L. H.; Balet, L.; Francardi, M.; Gerardino, A.; Fiore, A.; Gurioli, M. Near-field imaging of coupled photonic-crystal microcavities. *Appl. Phys. Lett.* **2009**, *94*, 151103.

(23) Caselli, N.; Intonti, F.; Riboli, F.; Vinattieri, A.; Gerace, D.; Balet, L.; Li, L.; Francardi, M.; Gerardino, A.; Fiore, A.; Gurioli, M. Antibonding ground state in photonic crystal molecules. *Phys. Rev. B: Condens. Matter Mater. Phys.* **2012**, *86*, 035133.

DOI: 10.1021/acsphotonics.5b00422
ACS Photonics 2015, 2, 1636−1643

(24) Caselli, N.; Intonti, F.; Riboli, F.; Gurioli, M. Engineering the mode parity of the ground state in photonic crystal molecules. *Opt. Express* **2014**, *22*, 4953−4959.
(25) Chien, F.-S.; Tu, J.; Hsieh, W.-F.; Cheng, S.-C. Tight-binding theory for coupled photonic crystal waveguides. *Phys. Rev. B: Condens. Matter Mater. Phys.* **2007**, *75*, 125113.
(26) Vignolini, S.; Intonti, F.; Riboli, F.; Wiersma, D. S.; Balet, L.; Li, L. H.; Francardi, M.; Gerardino, A.; Fiore, A.; Gurioli, M. Polarization-sensitive near-field investigation of photonic crystal microcavities. *Appl. Phys. Lett.* **2009**, *94*, 163102.
(27) Intonti, F.; Riboli, F.; Caselli, N.; Abbarchi, M.; Vignolini, S.; Wiersma, D.; Vinattieri, A.; Gerace, D.; Balet, L.; Li, L.; Francardi, M.; Gerardino, A.; Fiore, A.; Gurioli, M. Young's type interference for probing the mode symmetry in photonic structures. *Phys. Rev. Lett.* **2011**, *106*, 143901.
(28) Caselli, N.; Intonti, F.; La China, F.; Riboli, F.; Gerardino, A.; Bao, W.; Weber-Bargioni, A.; Li, L.; Linfield, E.; Pagliano, F.; Fiore, A.; Gurioli, M. Ultra-subwavelength phase sensitive Fano-imaging of localized photonic modes. *Light: Sci. Appl.* **2015**, *4*, e32610.1038/lsa.2015.99.
(29) Schnell, M.; Garcia-Etxarri, A.; Huber, A.; Crozier, K.; Aizpurua, J.; Hillenbrand, R. Controlling the near-field oscillations of loaded plasmonic nanoantennas. *Nat. Photonics* **2009**, *3*, 287−291.
(30) Burresi, M.; Engelen, R.; Opheij, A.; Van Oosten, D.; Mori, D.; Baba, T.; Kuipers, L. Observation of polarization singularities at the nanoscale. *Phys. Rev. Lett.* **2009**, *102*, 033902.

NOTE ADDED AFTER ASAP PUBLICATION

This paper was originally published ASAP on October 28, 2015. Due to a production error, Niccolò Caselli was omitted from the author list. The corrected version was reposted on October 29, 2015.

DOI: 10.1021/acsphotonics.5b00422
ACS Photonics 2015, 2, 1636−1643